Shape-recovery in organic solvents of water-responsive cellulose nanofiber actuators

Lisa Lopes da Costa, Céline Moreau, Denis Lourdin, Bernard Cathala, Ana Villares

Cellulose (2023) 30:5811–5824
https://doi.org/10.1007/s10570-023-05230-8

ORIGINAL RESEARCH

Shape-recovery in organic solvents of water-responsive cellulose nanofiber actuators

Lisa Lopes da Costa · Céline Moreau · Denis Lourdin · Bernard Cathala · Ana Villares

Received: 16 August 2022 / Accepted: 25 April 2023 / Published online: 13 May 2023

Abstract In this work, we have prepared films based on cellulose nanofibers (CNFs) that mimic plant responsiveness to water by shape-changing. Film twisting was achieved by creating an asymmetrical expansion through a gradient of carboxylate groups within the CNF film thickness. We present the characterization of pristine and modified CNFs, and their swelling and mechanical performances when conditioned into films. The immersion in water and organic solvents (isopropanol, ethanol, DMSO, acetonitrile, and cyclohexane) allowed controlling the asymmetrical expansion. Hence, film twisting is triggered when immersed in water and their shape recoveries were accomplished by dipping them in organic solvents. We investigated the main physicochemical interactions between the different CNFs and solvents governing film expansion. This work leaves the door open for the design of biomimetic cellulose-based materials for soft robotics, building materials, and electronic applications.

Keywords Cellulose nanofibers · Carboxymethylation · Film · Actuator · Twisting · Stimuli-responsive

Introduction

Biological systems display highly ordered architectures from nano- to macroscale using elementary building blocks from a bottom-up approach. Besides, they are multi-functional, environmentally adaptive, and biodegradable (Srinivasan et al. 1991). High recent attention in material science now stands on innovative structures that are based on natural resources and follow the inherent features of biological systems (Duan et al. 2017; Ganewatta et al. 2021; Markstedt et al. 2019; Mulakkal et al. 2018). New kinds of materials that respond to stimuli by shape-changing were developed as similarly observed in the plant kingdom, for example, the humidity-sensitive unfolding of pinecone scales (Dawson et al. 1997; Erb et al. 2013). These materials so-called actuators mainly consist of hierarchical structures that present a differential strain upon external stimuli governing the material movement in a bi- or tri-dimensional space (Burgert et al. 2016; Duigou et al. 2017; Chen et al. 2022).

Highly abundant on Earth, cellulose fibers are an ideal candidate to elaborate those materials of interest thanks to their accessible hydroxyl groups enabling large water uptake and their remarkable mechanical

Supplementary Information The online version contains supplementary material available at https://doi.org/10.1007/s10570-023-05230-8.

L. Lopes da Costa (✉) · C. Moreau · D. Lourdin · B. Cathala · A. Villares
UR1268 BIA, INRAE, 44316 Nantes, France
e-mail: lisa.lopes-da-costa@inrae.fr

properties (Huber et al. 2011). Moreover, cellulose nanofibers (CNFs), obtained by mechanical fibrillation of the fiber, are a great starting material to design actuators. CNFs have a high aspect ratio (3–5 nm in width and upwards of several micrometers in length) facilitating the intercalation of water molecules in the cellulose network, and as a consequence enhanced actuation performances (Zhang et al. 2016a; Kuang et al. 2019; Wei et al. 2021; Yang et al. 2021). Hence, Wang et al. (2015) fabricated a single-layer CNF film subjected to an asymmetrical stimulus. The water vapor is deposited unidirectionally under the film to create a humidity gradient through the thickness of the film. The film bent towards the less moisturized side and then returned to its original shape when water vapor was not directed.

A myriad of other CNF-based actuators responding to different stimuli such as temperature, electricity, magnetic field, and light have been developed over the last two decades but it turns out that in most of them, cellulose is used as a tuning element for mechanical properties (Zhao et al. 2018, 2020; Wang et al. 2019; Peng et al. 2020; Zhou et al. 2020; Liang et al. 2020; Chen et al. 2022). Our approach is to design actuators where cellulose is responsible for the motion response without being associated with synthetic polymers. To meet today's environmental challenges, the development of new materials must take into account the initial use of raw resources to its end-of-life (Duchemin 2022). Here, the objective is to extend cellulose applicability in the actuator field but also to avoid multi-component materials that may lead to delamination or phase separation issues (Faruk et al. 2012) and biodegradation or recycling difficulties (Duchemin 2022).

Therefore, new functional groups sensitive to external stimuli can be implemented on the CNF surface, and graduated films can then be manufactured from layers with different degrees of functionality to achieve the desired effect (Chen et al. 2022). In previous works, we prepared a bilayer film containing functionalized CNFs with pH-responsive groups: on one side, carboxylic acid groups via TEMPO oxidation, and on the other side, amino groups via TEMPO oxidation followed by a peptide coupling. Once dipped into a low pH solution, the amino groups were protonated, the electrostatic repulsion between the positive charges led to the swelling of the layer, and the film bent towards the carboxylic layer. The inverse mechanism for the carboxylic layer was observed when the film was immersed in a high pH solution (Chemin et al. 2020). A key point in the actuation of these bilayers is the swelling, and thus the interaction with solvents. To extend our understanding of the interactions with cellulosic structures, in this work, we have studied the swelling behavior of bilayer films composed of a passive and active layer subjected to different solvents. Water and organic solvents (isopropanol (IPA), ethanol (EtOH), dimethyl sulfoxide (DMSO), acetonitrile (ACN), and cyclohexane) have different physico-chemical properties allowing consequent structural changes of the different CNF layers. We focused on carboxymethylated cellulose nanofibers (CMCNFs) rather than TEMPO-oxidized CNF due to its timeliness of functionalization (Im et al. 2018). Moreover, carboxylic groups on TOCNFs are grafted on C6 of the anhydroglucose unit of cellulose (Saito and Isogai 2004; Saito et al. 2005) whereas carboxymethylation occurs on all hydroxyl groups (Kono et al. 2016). These two chemical modifications result in different structural patterns. CMCNFs exhibited a less crystalline structure which can considerably influence the solvent uptakes of the fiber (Mohkami and Talaeipour 2011). Thus, using CMCNFs could give interesting information regarding the conditions to achieve reversibility.

After characterizing the pristine CNFs and CMCNFs (degree of substitution, crystallinity, fibril morphology), we evaluated the influence of water uptake of single-layer films, containing either pristine or modified CNFs, on their swelling and mechanical performances, which are the key parameters driving actuation. Then, we succeed in triggering the bending of bilayer films in water and then controlling their shape recovery with organic solvents (isopropanol, ethanol, acetonitrile, dimethyl sulfoxide, and cyclohexane). The main physico-chemical interactions between cellulose and solvents were investigated by conducting multiple linear regressions.

Materials and methods

Materials

CNFs *Exilva P 01-V (10% w/w)* were kindly provided by Borregaard (Sarpsborg, Norway). Monochloroacetic acid (MCA), sodium hydroxide (NaOH), and

hydrochloric acid (HCl) were purchased from Sigma Aldrich. Acetonitrile and dimethyl sulfoxide were purchased from Merck, cyclohexane from Fluka Chemicals, ethanol from Carlo Erba Reagents, and isopropanol (IPA) from VWR. Water was purified by the Millipore Milli-Q purification system (18.2 MΩ).

Carboxymethylation

500 mg of CNFs were impregnated with MCA dissolved in IPA for 1 h at room temperature. Five MCA/anhydroglucose (AGU) molar ratios were tested: 0.17, 0.26, 0.35, 0.52, and 0.69. In parallel, NaOH was solubilized in IPA in a round bottom flask at 60 °C (NaOH/MCA molar ratio = 4). The CNF dispersion was then added to the flask and, was stirred for 1 h at 70 °C. The resulting dispersion was purified via vacuum filtration through polyvinylidene fluoride (PVDF) membranes (pore size 0.22 µm) with Milli-Q water, then an HCl solution (0.1 M), and finally water until the pH reached 7.

Film fabrication

The CNF films were prepared by vacuum filtration at 50 mbar through PVDF membranes (pore size 0.22 µm, diameter 47 mm). For the single-layer films, an aqueous dispersion containing CNFs (2.5 g L^{-1}) or carboxymethylated CNFs (CMCNFs, 2.5 g L^{-1}) was filtrated for 30 min. Regarding the bilayer films, a CNF dispersion was filtered for 30 min, then a CMCNF dispersion was cast on top of the first CNF layer and was also filtrated for 30 min. All films were then dried between two layers of Whatman® qualitative filter papers (Grade 1, diameter 47 mm) pressed by a weight of 500 g on the films in a desiccator at room temperature for 48 h. Afterward, the films were weighed and their thickness was measured with a Mitutoyo digimatic micrometer. The density was calculated as represented below:

$$\mathrm{d} = \frac{\mathrm{m}}{\pi r^2 t} \tag{1}$$

where m, r, and t are respectively the weight, radius, and thickness of the dried films.

To perform the actuation tests, films were cut into four rectangles of 6 × 24 mm.

Characterization

Fourier transform infrared (FTIR)

Infrared spectra were collected from KBr pellets containing freeze-dried CNFs and CMCNFs on FTIR Nicolet iS50 spectrometer (Thermo Scientific) with 4 cm^{-1} resolution after 200 continuous scans from 400 to 4000 cm^{-1}.

Carboxylic acid group content

Samples were acidified with 0.01 M HCl. The yield of carboxymethylation was quantified by conductometric titration with 0.01 M NaOH solution by a TIM900 titration manager and a CDM749 conductivity cell (Metrohm). The degree of substitution (DS) was calculated as (Abitbol et al. 2013; Beck et al. 2015):

$$DS = \frac{162\left(V_{eq2} - V_{eq1}\right)C_{\mathrm{NaOH}}}{m - M\left(V_{eq2} - V_{eq1}\right)C_{\mathrm{NaOH}}} \tag{2}$$

where V_{eq1} and V_{eq2} are the equivalence volumes of NaOH (L), C_{NaOH} the concentration of NaOH (mol L^{-1}), m the dried weight of CNFs (g), M the molecular weight of the carboxymethyl group, and 162 the molecular weight of AGU (g mol^{-1}).

X-ray diffraction (XRD)

X-ray diffractograms of freeze-dried CNFs and CMCNFs were monitored by recording X-ray diffraction diagrams every 10 min on a Bruker D8 Discover diffractometer with a Ni-filtered Cu Kα1 radiation (Cu K α1 = 1.5405 Å), produced in a sealed tube at 40 kV, and 40 mA, selected and parallelized using a Gobël mirror parallel optics system and collimated to produce a 500 µm beam diameter. X-ray diffraction data were collected using a Bruker Vantec 500 two-dimensional detector. Crystallinity was calculated from the XRD patterns of cellulose according to the method of Segal et al. (1959).

$$Crystallinity\,(\%) = \frac{I_{200} - I_{am}}{I_{200}} \times 100 \tag{3}$$

where I_{200} is the maximum intensity of the (200) peak and I_{am} is the minimum intensity between the (200) and (110) peaks corresponding to the amorphous part of cellulose.

Scanning transmission electron microscopy (STEM)

CNF and CMCNF dispersions were diluted to 0.1 g L^{-1} and deposited on freshly glow-discharged carbon-coated electron microscope grids (200 mesh, Delta Microscopies, France). Water excess was removed by blotting (Whatman filter paper). The grids were dried overnight in air at ambient temperature and then coated with platinum layer by an ion-sputter coater (thickness = 0.5 nm). The grids were observed with a Quattro Scanning electron microscopy (Thermo Scientific) with a STEM detector, working at 10 kV under a low vacuum (100 Pa).

Solvent uptake quantification

Disc-shaped films were cut into squares of 24 × 24 mm^2. The dry films were hooked and weighed, then immersed in the solvent for 1 min and weighed again. The swelling expressed as the weight of absorbed solvent per the weight of the dry film (*Sw*) was calculated following this equation:

$$Sw = \frac{(m_w - m_d)}{m_d} \quad (4)$$

where m_w and m_d are respectively the weight of the wet and dry film (mg).

The molar swelling expressed as the number moles of solvent per anhydroglucose unit (*nSw*) was calculated following this equation:

$$nSw = \frac{162(m_w - m_d)}{M_s m_d} \quad (5)$$

where 162 is the molecular weight of AGU (g mol^{-1}) and M_s is the molecular weight of the solvent (g mol^{-1}) (Table S1).

Environmental scanning electron microscopy (ESEM)

Cross-sectional images of CNF or CMCNF films were acquired employing an ESEM instrument (Thermo Scientific) under different relative humidity by varying the pressure from 232 to 950 Pa at an acceleration voltage of 15 kV.

Dynamical mechanical analysis (DMA)

The dynamic mechanical properties with water activity of CNF or CMCNF films were determined with a Dynamic Mechanical Analyser (DTMA MkIV, Rheometric Scientific, US) equipped with a homemade humidity conditioning system. Tests were conducted on rectangular-shaped strip samples (10 × 6 mm) in the tensile mode with a constant strain amplitude of 0.1%, and a constant load force of 0.1 N at 20 °C. Relative humidity (RH) sweeps were recorded following this program: 16 h overnight equilibrium to dry the film at 5% RH, then 6 h at 50%, and finally 6 h at 70%. The DMA system can be flipped from bottom to top in order to measure the samples immersed in water and IPA. Recordings of the specimens were taken following this procedure: 10 min air equilibrium, then 30 min immersion in water or IPA.

Results and discussion

Carboxymethylation

Carboxymethylation was performed to introduce new stimuli-responsive functionalities on the CNF surface, herein, carboxymethyl groups (Fig. 1a). To avoid the full dissolution of cellulose chains, fibers were impregnated with monochloroacetic acid (MCA) before the alkaline conditions (Wågberg et al. 2008). Both starting CNFs and CMCNFs showed the common FTIR profile of cellulose fibers (Fig. 1b). The following bands are detected: 3774–3007 cm^{-1} (–O–H stretching vibration), 3007–2790 cm^{-1} (C–H stretching), 1650 cm^{-1} adsorbed water, 1367 cm^{-1} (CH_3 deformation), and 1201–1026 cm^{-1} (ether bonding) (Oh et al. 2005; Schwanninger et al. 2004). However, CMCNF spectra showed an extra band at 1730 cm^{-1} corresponding to the carbonyl bond stretching of the protonated carboxylic acid groups (da Silva Perez et al. 2003).

To achieve different degrees of substitution (DS), we performed carboxymethylation reactions with five different MCA/AGU molar ratios from 0.17 to 0.69. The DS of each reaction was quantified by conductometric titration (Fig. S1), according to the Eq. (2).

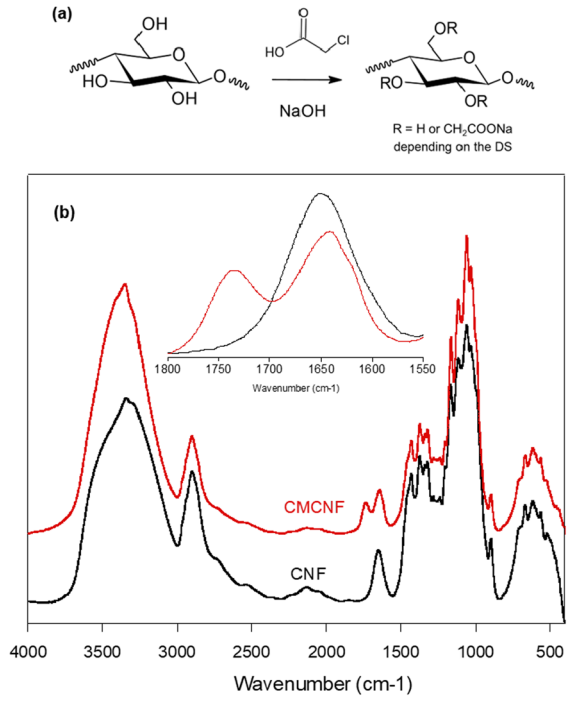

Fig. 1 **a** Reaction scheme of carboxymethylation, **b** FTIR spectra in absorbance of CNFs and CMCNFs. The inset shows the 1800–1550 cm^{-1} region

The plot in Fig. 2a of the DS as a function of MCA/AGU ratio shows that the reaction was linearly reliable to the amount of MCA (DS of 0.02, 0.09, and 0.17 for respectively a ratio of 0.17, 0.52, and 0.69).

X-ray diffraction measurements were performed to analyze the crystalline organization of CNFs and CMCNFs with a DS of 0.02, 0.09, and 0.17 (respectively CMCNF2, CMCNF9, and CMCNF17) (whole diffractograms are shown in Fig. S2). The CNF diffractograms are consistent with the cellulose I X-ray patterns, showing peaks at 14.5°, 16.2° and 22.2°, corresponding to Miller indices of ($\bar{1}$10), (110) and (200), respectively (Segal et al. 1959; French and Santiago Cintrón 2013; Ju et al. 2015). However, as the DS increased (CMCNF9), a different X-ray pattern was observed, suggesting the disruption of the cellulose I crystalline structure. The diffractograms pointed to the formation of cellulose II in CMCNF9 (peaks at 20.2° and 22.3° corresponding to Miller indices of (110) and (020), respectively (French and Santiago Cintrón 2013; French 2014); and a high loss of crystallinity for higher DS (CMCNF17). Figure 2b shows a starting crystallinity of 63% for CNFs that was maintained for CMCNF2 (60%), and then significantly reduced for CMCNF9 and CMCNF17, accordingly to the increase of DS (respectively 35 and 17%).

The fiber morphology was observed by STEM. Figure 2c shows starting CNFs consisting of fibril aggregates (until 92 nm of diameter) and some individual nanofibers with an average diameter of 17 nm in agreement with characteristic CNF dimensions (Wang et al. 2021). The fibrillar network for CMCNF2 remained unchanged (Fig. 2d). By increasing DS (CMCNF9), new individual fibrils appeared (Fig. 2e) until reaching a highly nanofibrillated network for CMCNF17 with a fibril diameter average of 15 ± 4 nm (Fig. 2f).

During the reaction, the alkaline treatment with NaOH swelled the fibrils facilitating the etherification of the hydroxyls by carboxymethyl groups. Then, fibrillation was boosted by the osmotic repulsion due to the overlap of the electric double layers (Baati et al. 2017; Boufi and Chaker 2016). This fiber detachment was reflected by the disruption of the crystalline regions giving rise to the amorphization of cellulose (Chen et al. 2013; Im et al. 2018). From the DS studied, CMCNF2 and CMCNF9 were selected as starting materials for the film preparation whereas CMCNF17 was discarded because of its too low crystallinity and high fiber disruption.

Water uptake in cellulose films

We first determined the water uptake of single-layer films of CNFs or the different CMCNFs. The visual aspect of the films is shown in Figure S3. Films showed a clear increase in water uptake with increasing DS: swelling ratios (*Sw*) of 2.45 ± 0.18 for CNFs, 3.99 ± 0.48 for CMCNF2, and 9.27 ± 0.3 for CMCNF9. At the molecular level, water uptake in cellulose is governed by the interactions between water molecules and the hydroxyl groups. The presence of negative charges on CMCNFs facilitates the separation of elementary fibrils, which increases the accessible surface and the water adsorption. Thus, water uptake is more substantial with a higher surface charge, and thus DS. Fält et al. (2003) described that carboxymethylated cellulose swelled more in water than unmodified cellulose due to the negative charges, in agreement with our results.

In order to get more insight into the response of films to water stimuli, the thickness increase of

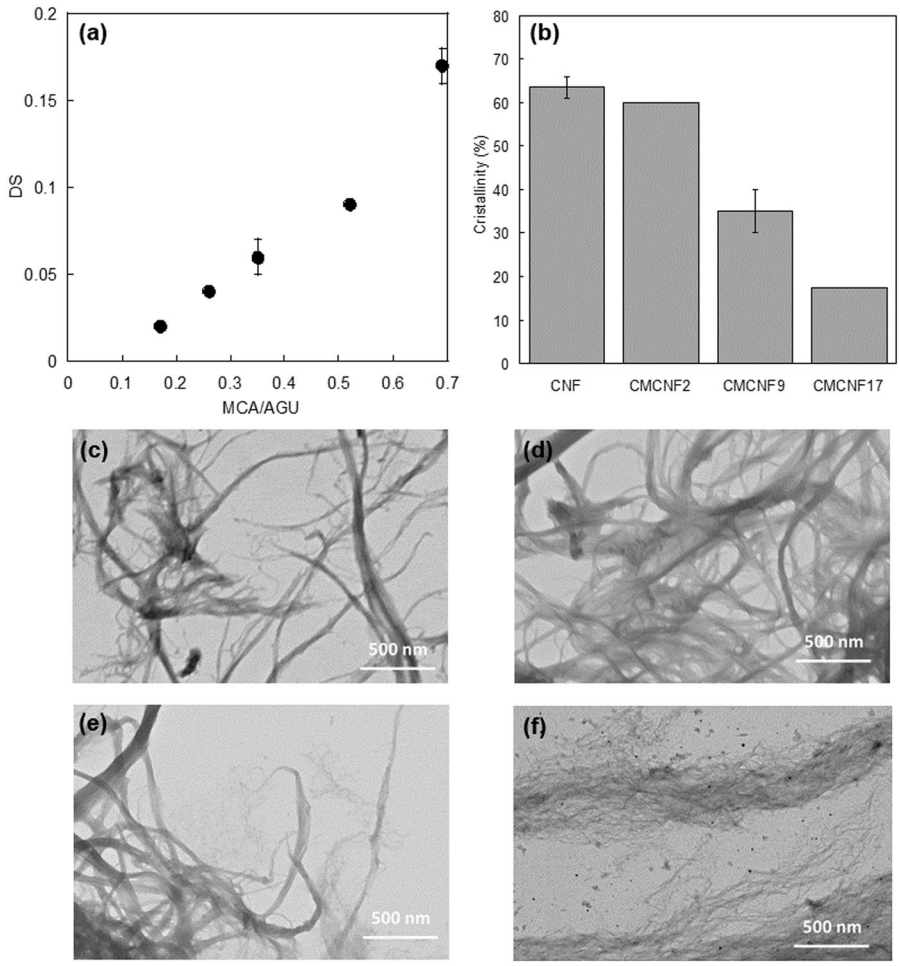

Fig. 2 **a** Influence of MCA/AGU molar ratio on the DS. **b** Influence of DS on the crystallinity, STEM images of **c** CNFs, **d** CMCNF2, **e** CMCNF9, and **f** CMCNF17

single-layer films was monitored by ESEM in controlled humidity environment. ESEM permits to observe samples at different relative humidity (RH) by varying the pressure in the microscope specimen chamber (Mayeen et al. 2018). Therefore, the influence of moisture on film morphology can be examined at the microscale level. Figure 3a–d show cross-sectional ESEM images of CNFs and CMCNF9 films at 25 and 100% RH. Films exhibited average thicknesses of 20 ± 2 µm for CNFs and 11 ± 1 µm for CMCNF9 with an apparent density of 0.7 ± 0.1 g cm^{-3}. While the thickness of CNF film did not evolve with raising RH, the CMCNF9 film exhibited an important volume expansion at 100% RH.

Then, the effect of film hydration on mechanical properties was characterized by recording the storage modulus (*E'*) of CNF and CMCNF single-layer films by DMA at different relative humidity (from 5 to 70% RH, and fully immersed in water) (Fig. 3e). As expected, when RH increased, both CNF and CMCNF9 films showed a clear decrease in the storage modulus. At 5%, the CNF film exhibited an *E'* of 6.53 ± 0.41 GPa in agreement with literature (values varying from 1.2 to 21 GPa due to the interfibrillar arrangement (Benítez and Walther 2017; Mokhena et al. 2021)). For the CMCNF9 film, a lower *E'* was obtained (4.12 ± 0.26 GPa). The phenomenon drastically operated when the films were completely immersed in water (0.19 ± 0.02 GPa for CNF film and 0.01 ± 0.00 GPa for CMCNF9 film).

The increase of RH involved the progressive substitution of cellulose-cellulose to cellulose-water hydrogen bonding detangling the fibrillar network, and consequently entailing higher slippage performances (Benítez et al. 2013; Zhang et al. 2016b), which resulted in lower film stiffness. In the case of

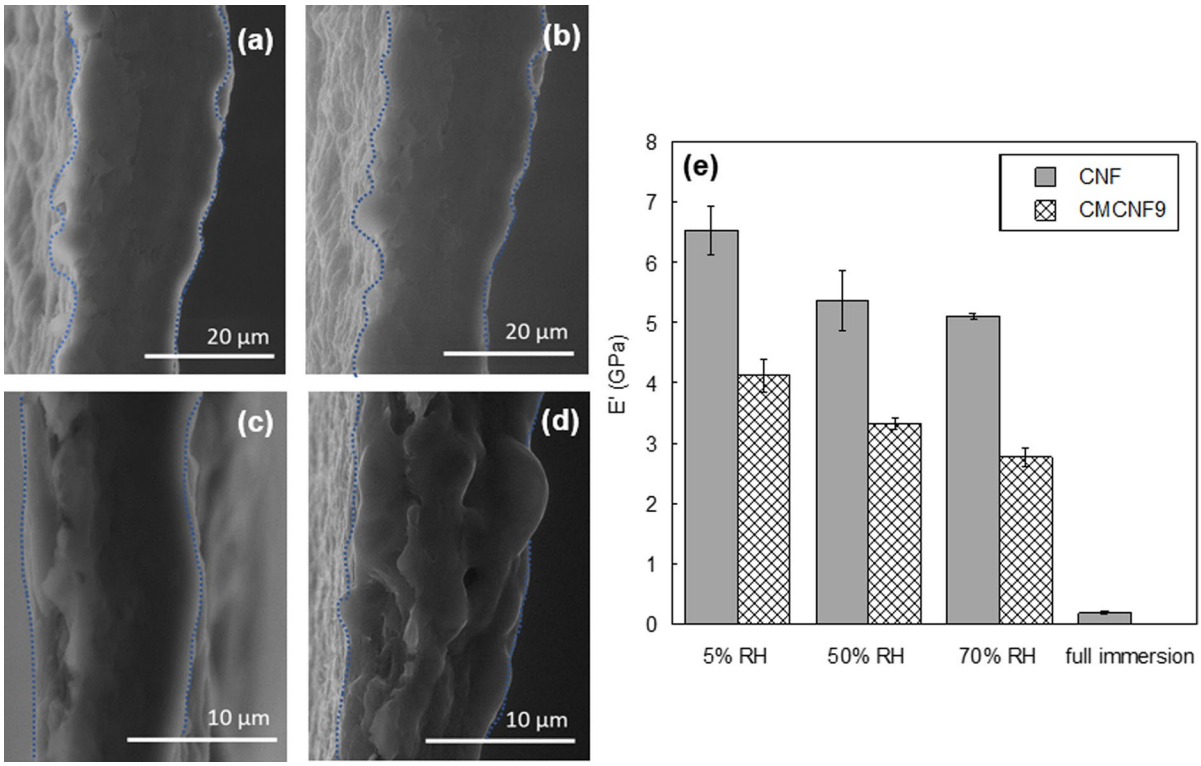

Fig. 3 Cross-sectional ESEM images of single-layer films at different RH of **a** CNF film at 25%, **b** CNF film at 100%, **c** CMCNF9 film at 25%, and **d** CMCNF9 film at 100%. Blue dotted lines represent the limits of film cross-sections, **e** Storage modules *E'* of CNF and CMCNF9 films at 5%, 50%, 70% RH, and in full immersion

CMCNF9 films, the lower storage modulus at the different humidity could be explained by its less cohesive structure as it has a stronger affinity with water.

Reversible actuation of bilayer cellulose films under water and IPA changes

Based on the different water uptake and mechanical properties, we prepared bilayer films composed of a first layer containing CNFs and a second layer composed of CMCNF2 or CMCNF9 by vacuum filtration, and we evaluated their bending performance. Films exhibited average thicknesses of 34 ± 4 µm with an apparent density of 0.7 ± 0.1 g cm^{-3} (Fig. S4a).

When bilayer films (rectangular-shaped strips, Fig. S4b) were immersed in water, they successfully twisted with the CMCNF layer on the outside, indicating the higher water uptake of the CMCNF layer (Fig. 4a, b). CNF/CMCNF2 and CNF/CMCNF9 films reached the same high twisted state within 30 s. After water immersion, the wet bilayer films were dipped in IPA. Surprisingly, different responses were obtained depending on the DS of the CMCNF layer. Thus, the CNF/CMCNF2 film did not show reversible actuation while CNF/CMCNF9 recovered slowly their initial shape within 5 min. After waiting 30 min, the response for both films remained unchanged.

In water, the CMCNF9 layer was highly swollen compared to the CNF layer. When the bilayer film was then immersed in IPA, the solvent acted as a dehydrating agent, bringing out all water molecules within the film (Capadona et al. 2008). In order to get more insight into the mechanism of the reversible actuation, and the different behavior of CMCNF2 and CMCNF9, we investigated the behavior of the single-layer films (CNFs, CMCNF2, and CMCNF9) in IPA compared to water. We evaluated the values of IPA uptake of each single-layer film expressed as the number of molecules of solvent per AGU to consider only the molecular interactions of the solvent with cellulose (*nSw*). Differently from water swelling, which was significantly different for CNF and

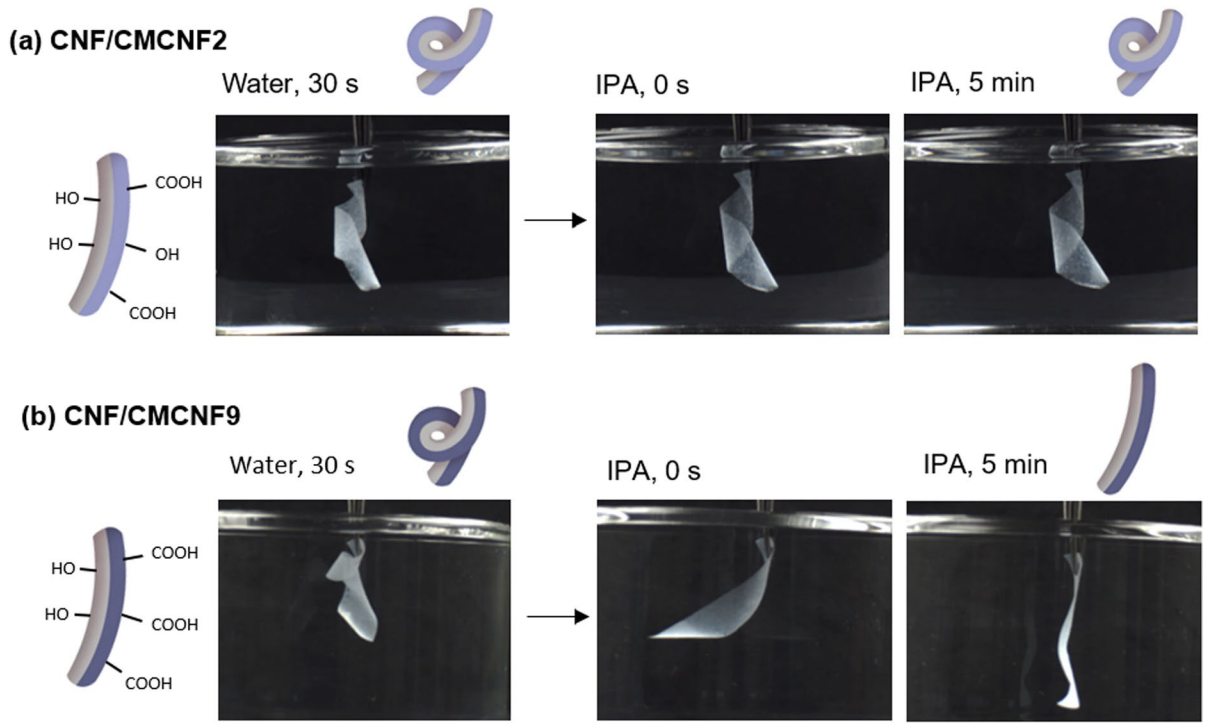

Fig. 4 Photographs showing the twisting in water followed by the shape recovery test in IPA of **a** CNF/CMCNF2 and **b** CNF/CMCNF9 bilayer films

CMCNF films (*nSw* of 22 ± 2 for CNFs, 35 ± 4 for CMCNF2, and 84 ± 3 for CMCNF9), IPA swelling was similar for CNF, CMCNF2, and CMCNF9 films. In addition, the IPA uptake was significantly lower than those of water (*nSw* of 4 ± 0 for CNFs, 7 ± 2 for CMCNF2, and 6 ± 1 for CMCNF9) (Fig. S5a). We also compared the storage modulus of CNF and CMCN9 films when immersed in IPA by DMA and they showed similar values of storage modulus at 5% RH (5.41 ± 0.05 GPa for CNF films and 4.31 ± 1.02 GPa for CMCNF9 films in IPA).

DMA measurements also allowed determining changes in the film length upon immersion in the liquid. In water, the relative elongations of CNF and CMCNF9 single layer films were 8.5 ± 0.0% and 11.2 ± 1.4%, respectively, while a shrinkage in IPA for both films was observed (− 0.7 ± 0.0% for CNF and − 0.8 ± 0.1% for CMCNF9 films).

Therefore, reversibility seemed to be driven by the difference in the absolute values of solvent uptake. The high deswelling of the CMCNF9 layer could trigger the reversibility of bending, and hence the CNF/CMCNF9 film recovered its initial shape. Differently, when the water uptake was close for both layers (CMCNF2 and CNFs), the immersion in IPA did not yield such a great difference in deswelling, and the bilayer remained bent. Therefore, we assumed that the difference in swelling of CMCNF9 between water and IPA is the driving force for full shape recovery.

Shape recovery in other solvents

Several solvents were tested to compare the mechanism of actuation in IPA: ethanol (EtOH) which is a polar protic solvent with a smaller steric hindrance than IPA, DMSO, and acetonitrile (ACN), which are polar aprotic solvents with different molar volumes, and cyclohexane, which is a non-polar solvent. We focused only on the behavior of the CNF/CMCNF9 bilayer film.

CNF/CMCNF9 films were first immersed in water, and then in the different solvents. DMSO, EtOH, and ACN proved their efficiency to enable the reverse movement of the films (Fig. 5a–c) meanwhile cyclohexane did not interact with the films leaving them in a twisted shape (Fig. 5d). Besides, the film

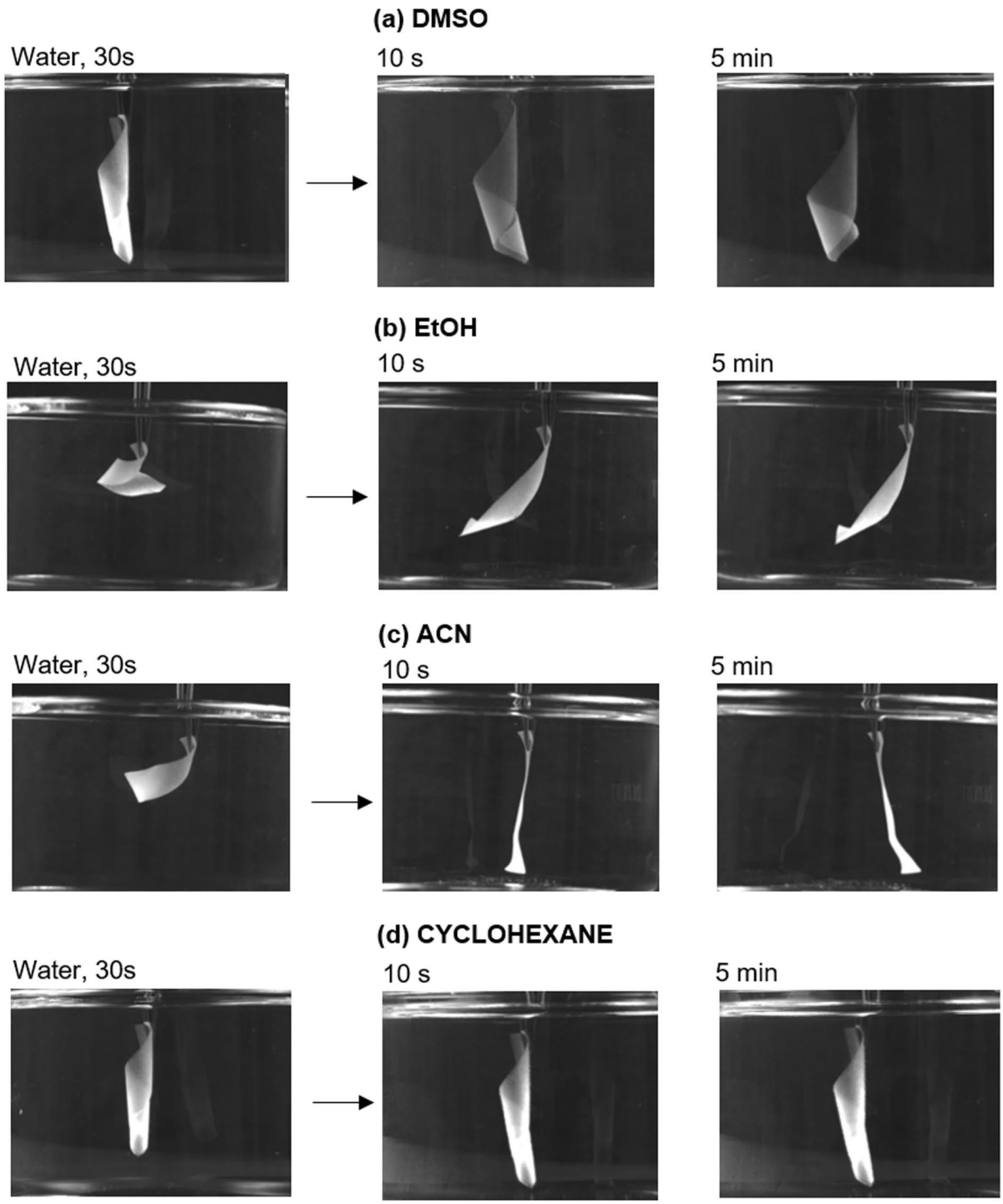

Fig. 5 Photographs showing the shape recovery test of CNF/CMCNF9 bilayer film in **a** DMSO, **b** EtOH, **c** ACN, and **d** cyclohexane

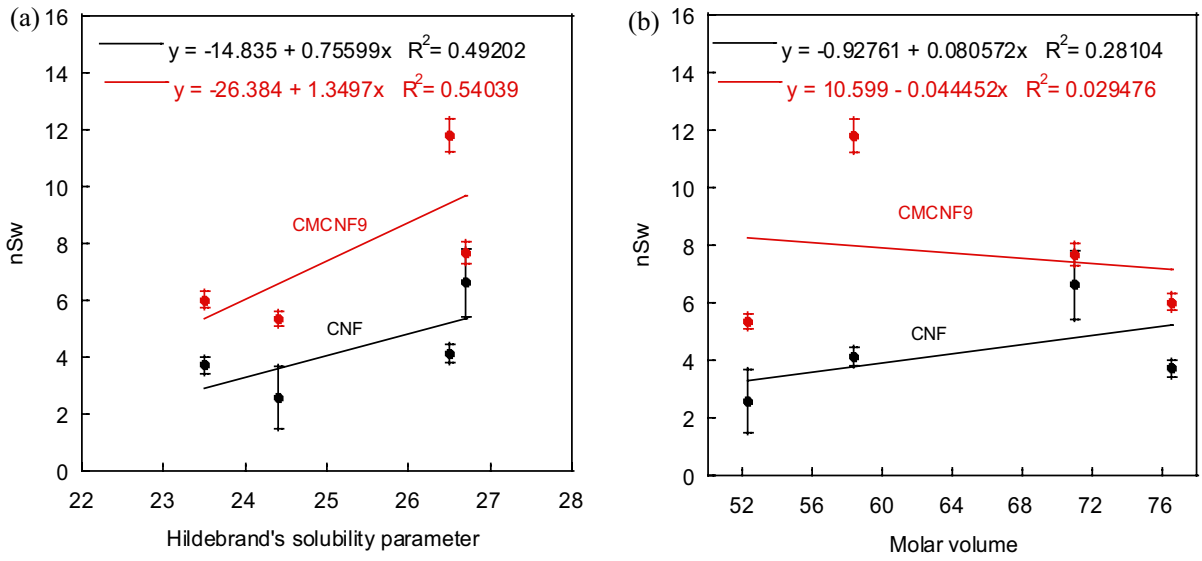

Fig. 6 *nSw* of CNF and CMCNF9 single-layer films as a function of (**a**) $\delta_{Hildebrand}$ and (**b**) V_s parameters

in DMSO, EtOH, and ACN showed different kinetics and shape recovery extent. In DMSO and EtOH, films followed a slow path similar to IPA (around 5 min) but we observed an incomplete unbending (Fig. 5a, b). ACN led to an ultrafast shape recovery within 10 s (Fig. 5c). In the case of cyclohexane, water might be trapped within the film, as this solvent is non-miscible with water, making impossible the penetration of water molecules. In contrast, polar solvents succeeded to replace water in the film, shrinking the CMCNF layer, and driving the backward movement. The differences between solvents suggested that they did not only play a role as dehydrating agents but their nature and properties impacted the extent and rate of shape recovery. Investigation at the molecular level was therefore required to better understand which physicochemical interactions govern swelling and how these parameters influence the time response of shape-recovery.

Few articles in the literature address the cellulose-solvent molecular interactions in non-aqueous liquid media even though cellulose dissolution is particularly an important step to process it. The work from Cranston's team probed the swelling of thin cellulose nanocrystal films in different solvents (Reid et al. 2016) and correlated these results with Hildebrand solubility parameters ($\delta_{Hildebrand}$). $\delta_{Hildebrand}$ is a useful tool to predict the polymer-solvent interactions because it comprises dispersive, polar, and hydrogen bonding components. This parameter is related to the cohesive energy density, that is the energy needed to completely remove unit volume molecules from their neighbors to infinite separation, herein, intra and intermolecular hydrogen bonds of cellulose (Venkatram et al. 2019). Figure 6a shows the *nSw* values for CNF and CMCN9 films in the different solvents versus $\delta_{Hildebrand}$ (values reported in Fig. S5b and Table S1) to assess the efficiency of this descriptor for the correlation between swelling and cellulose-solvent interactions and, we obtained a correlation coefficient of 0.49 for CNFs and 0.54 for CMCNF9, which is a reasonable interdependence. The dependency against the solvent molar volume (V_s) was also evaluated and a very poor correlation resulted (Fig. 6b). We investigated other parameters, including the relative polarity (*RP*), dielectric constant at 25 °C (ε_r), Van der Waals volume (V_W), hydrophobic character (Log P_s), dispersive, polar and hydrogen bonding contributions from Hansen model (δ_d, δ_p, δ_h, respectively), basicity (β_s), and dipolarity (π_s*). Values are reported in Table S1 (Barton 1991; El Seoud et al. 2008; Fidale et al. 2008; Smallwood 2012).

We performed single correlations between solvent parameters and swelling, and in all cases, the correlation was not clear (Tables S2 and S3), which suggested that cellulose swelling is a complex process

Table 1 Selected correlations of *nSw* of the CNF film with two solvent parameters

	Coupled parameters	Linear regressions	R^2	ΣQ^2
CNF	β_s; *log Ps*	$nSw = -0.01\ (\pm 0.10) + 4.52\ (\pm 0.14)\ \beta_s - 2.37\ (\pm 0.05)\ \log P_s$	0.9992	0.0024
	β_s; π_s*	$nSw = -3.43\ (\pm 1.28) + 5.24\ (\pm 1.33)\ \beta_s + 6.07\ (\pm 1.16)\ \pi_s$*	0.9752	0.2140
	V_s; $\delta_{Hildebrand}$	$nSw = -24.36\ (\pm 8.59) + 0.10\ (\pm 0.04)\ V_s + 0.88\ (\pm 0.30)\ \delta_{Hildebrand}$	0.9226	0.6684
	$\delta_{Hildebrand}$; δ_d	$nSw = -38.48\ (\pm 0.93) + 0.93\ (\pm 0.41)\ \delta_{Hildebrand} + 0.49\ (\pm 0.49)\ \delta_d$	0.8639	1.1743
	V_s; π_s*	$nSw = -3.73\ (\pm 4.79) + 0.07\ (\pm 0.07)\ V_s + 5.27\ (\pm 3.30)\ \pi_s$*	0.7976	1.7464
	ε_r; V_W	$nSw = -3.38\ (\pm 4.96) + 0.06\ (\pm 0.07)\ \varepsilon_r + 2.41\ (\pm 1.88)\ V_W$	0.7162	2.4493

R^2 is the correlation coefficient of the linear regressions and ΣQ^2 the sum of the residues on two solvent parameters

including various parameters and cannot be explained by a single solvent property. Multiple linear regressions were carried out in order to better estimate cellulose-solvent interactions with two solvent parameters:

$$nSw = a + bp_{s1} + cp_{s2} \tag{6}$$

where p_{s1} and p_{s2} are the solvent parameters, and a, b, and c are constants.

As water has a completely different behavior, it was excluded from the regressions. Tables 1 and 2 review the correlations between *nSw* and two solvent parameters for the CNF and CMCNF9 films, respectively.

The main contributions of solvent parameters for CNF differed from those for CMCNF9. The swelling of CNF is subjected to the following coupled parameters: β_s, log P_s, π_s*, V_s, and $\delta_{Hildebrand}$, while the swelling of CMCNF9 is dominated by $\delta_{Hildebrand}$, *RP*, and δ_h ($R^2 > 0.90$). The manifestation of $\delta_{Hildebrand}$ in both celluloses evidences the effectiveness of using this descriptor to study cellulose-solvent interactions. For CNF, the driving force for swelling relies on the ability of the solvent molecules to penetrate the fiber interstices, to receive protons, and to intercalate between polar and carbon zones (affinity conditions to surround cellulose fibers). The initial structure constrains the physico-chemical properties of the solvent. Differently, this steric hindrance barrier is lifted for CMCNF9. The presence of carboxymethyl groups disrupts the fiber structure and the parameters relating to solvent molecular size, such as the molar volume, did not contribute to swelling. On the other hand, the carboxylic acid groups exacerbate the formation of hydrogen bonding and polar interactions, which was reflected by the contribution of *RP* and δ_h.

These results demonstrated that the introduction of carboxymethyl groups impacted not only the cellulose supramolecular arrangement but also the interactions with solvents. Therefore, playing with the degree of functionality and various solvent provides the control of actuation.

Conclusion

In this work, we combined carboxylated and non-modified cellulose nanofibers to fabricate bilayer films that bend when immersed in water. The

Table 2 Selected correlations of *nSw* of the CMCNF9 film with two solvent parameters

	Coupled parameters	Linear regressions	R^2	ΣQ^2
CMCNF9	$\delta_{Hildebrand}$;*RP*	$nSw = -32.86\ (\pm 0.36) + 1.18\ (\pm 0.01)\ \delta_{Hildebrand} + 0.21\ (\pm 0.00)\ RP$	0.9999	0.0014
	$\delta_{Hildebrand}$; δ_h	$nSw = -31.33\ (\pm 14.53) + 1.40\ (\pm 0.57)\ \delta_{Hildebrand} + 0.12\ (\pm 0.06)\ \delta_h$	0.9052	2.3796
	$\delta_{Hildebrand}$; δ_d	$nSw = 11.86\ (\pm 28.70) + 1.07\ (\pm 0.67)\ \delta_{Hildebrand} - 0.80\ (\pm 0.49)\ \delta_d$	0.8741	3.1602
	$\delta_{Hildebrand}$; δ_p	$nSw = -25.26\ (\pm 17.77) + 1.43\ (\pm 0.70)\ \delta_{Hildebrand} - 0.12\ (\pm 0.08)\ \delta_p$	0.8540	3.6654
	β_s; δ_d	$nSw = 44.56\ (\pm 26.17) + 6.39\ (\pm 7.20)\ \beta_s - 1.06\ (\pm 0.67)\ \delta_d$	0.7515	6.2397
	β_s; $\delta_{Hildebrand}$	$nSw = -27.45\ (\pm 28.97) + 3.93\ (\pm 9.01)\ \beta_s + 1.28\ (\pm 1.15)\ \delta_{Hildebrand}$	0.6141	9.6913

R^2 is the correlation coefficient of the linear regressions and ΣQ^2 the sum of the residues on two solvent parameters

presence of carboxylate groups favored the water uptake, and the greater expansion of this layer compared to the unmodified CNF layer facilitated film bending. Actuation was achieved even if the CMCNF was weakly charged (DS of 0.02); however, rapid liquid exchanges between water and the organic solvent (IPA, EtOH, DMSO, ACN), and high deswelling of the active layer were required to achieve reversibility. Films immersed showed irreversible behavior in cyclohexane and partial reversibility in DMSO and EtOH. In ACN and IPA, films completely recovered their original shape. This work opens the road for all-cellulose soft actuators and brings new opportunities to develop programmable materials from CNF for soft robotics, building materials, and electronic applications.

Acknowledgments The authors gratefully thank the financial support of Région Pays de la Loire and Transform Division from the French National Research Institute for Agriculture, Food and Environment. Theauthors acknowledge the Bioresources, Imaging, Biochemistry, and Structure (BIBS)platform of INRAE for the access to microscopy facilities (Bruno Novales) andX-ray diffraction (Bruno Pontoire). Anne-Laure Reguerre is acknowledged for theexcellent technical support for image acquisition and treatment. We gratefullyacknowledge Borregaard for kindly supplying the cellulose nanofibers.

Author contributions LL: Conceptualization, investigation, discussion, writing—original draft, writing—review and editing. CM: Discussion, writing—review and editing. DL: Investigation, discussion, writing—review and editing. BC: Discussion, Writing—review and editing. AV: Conceptualization, Investigation, discussion, funding acquisition, project administration, supervision, writing—review and editing. All authors have read and agreed to the published version of the manuscript.

Funding The authors gratefully thank the financial support of Région Pays de la Loire and Transform Division from the French National Research Institute for Agriculture, Food and Environment.

Data availability The datasets generated during the current study are available from the corresponding author on reasonable request.

Declarations

Conflict of interest The authors declare that they have no known competing financial interests or personal relationships that could have appeared to influence the work reported in this paper.

Ethics approval and consent to participate Not applicable.

Consent for publication Not applicable.

References

Abitbol T, Kloser E, Gray DG (2013) Estimation of the surface sulfur content of cellulose nanocrystals prepared by sulfuric acid hydrolysis. Cellulose 20:785–794. https://doi.org/10.1007/s10570-013-9871-0

Baati R, Magnin A, Boufi S (2017) High solid content production of nanofibrillar cellulose via continuous extrusion. ACS Sustain Chem Eng 5:2350–2359. https://doi.org/10.1021/acssuschemeng.6b02673

Barton AFM (1991) Handbook of solubility parameters and other cohesion parameters. pp 277–284

Beck S, Méthot M, Bouchard J (2015) General procedure for determining cellulose nanocrystal sulfate half-ester content by conductometric titration. Cellulose 22:101–116. https://doi.org/10.1007/s10570-014-0513-y

Benítez AJ, Walther A (2017) Cellulose nanofibril nanopapers and bioinspired nanocomposites: a review to understand the mechanical property space. J Mater Chem A 5:16003–16024. https://doi.org/10.1039/c7ta02006f

Benítez AJ, Torres-Rendon J, Poutanen M, Walther A (2013) Humidity and multiscale structure govern mechanical properties and deformation modes in films of native cellulose nanofibrils. Biomacromolecules 14:4497–4506. https://doi.org/10.1021/bm401451m

Boufi S, Chaker A (2016) Easy production of cellulose nanofibrils from corn stalk by a conventional high speed blender. Ind Crops Prod 93:39–47. https://doi.org/10.1016/j.indcrop.2016.05.030

Burgert I, Keplinger T, Cabane E et al (2016) Biomaterial wood: wood-based and bioinspired materials. Elsevier, Amsterdam

Capadona JR, Shanmuganathan K, Tyler DJ et al (2008) Stimuli-responsive polymer nanocomposites inspired by the sea cucumber dermis. Science 319:1370–1374. https://doi.org/10.1126/science.1153307

Chemin M, Beaumal B, Cathala B, Villares A (2020) Ph-responsive properties of asymmetric nanopapers of nanofibrillated cellulose. Nanomaterials 10:1–14. https://doi.org/10.3390/nano10071380

Chen Y, Wan J, Dong X, Ma Y (2013) Fiber properties of eucalyptus kraft pulp with different carboxyl group contents. Cellulose 206 20:2839–2846. https://doi.org/10.1007/S10570-013-0055-8

Chen W, Sun B, Biehl P, Zhang K (2022) Cellulose-based soft actuators. Macromol Mater Eng. https://doi.org/10.1002/mame.202200072

da Silva Perez D, Montanari S, Vignon MR (2003) TEMPO-mediated oxidation of cellulose III. Biomacromolecules 4:1417–1425. https://doi.org/10.1021/bm034144s

Dawson C, Vincent J, Rocca A (1997) How pine cone open. Nature 390:668

Duan J, Liang X, Zhu K et al (2017) Bilayer hydrogel actuators with tight interfacial adhesion fully constructed from natural polysaccharides. Soft Matter 13:345–354. https://doi.org/10.1039/c6sm02089e

Duchemin B (2022) The sustainability of phytomass-derived materials: thermodynamical aspects, life cycle analysis and research perspectives. Green Chem 24:2653–2679. https://doi.org/10.1039/d1gc03262c

Duigou A, Le, Requile S, Beaugrand J et al (2017) Natural fibres actuators for smart bio-inspired hygromorph biocomposites. Smart Mater Struct 26:125009. https://doi.org/10.1088/1361-665X/AA9410

El Seoud OA, Fidale LC, Ruiz N et al (2008) Cellulose swelling by protic solvents: which properties of the biopolymer and the solvent matter? Cellulose 15:371–392. https://doi.org/10.1007/s10570-007-9189-x

Erb RM, Sander JS, Grisch R, Studart AR (2013) Self-shaping composites with programmable bioinspired microstructures. Nat Commun 4:1–8. https://doi.org/10.1038/ncomms2666

Fält S, Wågberg L, Vesterlind EL (2003) Swelling of model films of cellulose having different charge densities and comparison to the swelling behavior of corresponding fibers. Langmuir 19:7895–7903. https://doi.org/10.1021/la026984i

Faruk O, Bledzki AK, Fink HP, Sain M (2012) Biocomposites reinforced with natural fibers: 2000–2010. Prog Polym Sci 37:1552–1596. https://doi.org/10.1016/j.progpolymsci.2012.04.003

Fidale LC, Ruiz N, Heinze T, El Seoud OA (2008) Cellulose swelling by aprotic and protic solvents: what are the similarities and differences? Macromol Chem Phys 209:1240–1254. https://doi.org/10.1002/macp.200800021

French AD (2014) Idealized powder diffraction patterns for cellulose polymorphs. Cellulose 21:885–896. https://doi.org/10.1007/S10570-013-0030-4

French AD, Santiago Cintrón M (2013) Cellulose polymorphy, crystallite size, and the Segal Crystallinity Index. Cellulose 20:583–588. https://doi.org/10.1007/s10570-012-9833-y

Ganewatta MS, Wang Z, Tang C (2021) Chemical syntheses of bioinspired and biomimetic polymers toward biobased materials. Nat Rev Chem 2021 511 5:753–772. https://doi.org/10.1038/s41570-021-00325-x

Huber T, Müssig J, Curnow O et al (2011) A critical review of all-cellulose composites. J Mater Sci 47:1171–1186. https://doi.org/10.1007/S10853-011-5774-3

Im W, Lee S, Rajabi Abhari A et al (2018) Optimization of carboxymethylation reaction as a pretreatment for production of cellulose nanofibrils. Cellulose 25:3873–3883. https://doi.org/10.1007/s10570-018-1853-9

Ju X, Bowden M, Brown EE, Zhang X (2015) An improved X-ray diffraction method for cellulose crystallinity measurement. Carbohydr Polym 123:476–481. https://doi.org/10.1016/j.carbpol.2014.12.071

Kono H, Oshima K, Hashimoto H et al (2016) NMR characterization of sodium carboxymethyl cellulose: substituent distribution and mole fraction of monomers in the polymer chains. Carbohydr Polym 146:1–9. https://doi.org/10.1016/j.carbpol.2016.03.021

Kuang Y, Chen C, Cheng J et al (2019) Selectively aligned cellulose nanofibers towards high-performance soft actuators. Extrem Mech Lett 29:100463. https://doi.org/10.1016/j.eml.2019.100463

Liang Y, Liu C, Xiu H et al (2020) Effect of 3D printing parameters on self-driven deformation characteristics of intelligent hydrogel actuators. ChemistrySelect 5:10367–10373. https://doi.org/10.1002/slct.202002424

Markstedt K, Håkansson K, Toriz G, Gatenholm P (2019) Materials from trees assembled by 3D printing: wood tissue beyond nature limits. Appl Mater Today 15:280–285. https://doi.org/10.1016/j.apmt.2019.02.005

Mayeen A, Shaji LK, Nair AK, Kalarikkal N (2018) Morphological characterization of nanomaterials. Charact Nanomater Adv Key Technol. https://doi.org/10.1016/B978-0-08-101973-3.00012-2

Mohkami M, Talaeipour M (2011) Investigation of the chemical structure of carboxylated and carboxymethylated fibers from waste paper via XRD and FTIR analysis. BioResources 6:1988–2003

Mokhena TC, Sadiku ER, Mochane MJ et al (2021) Mechanical properties of cellulose nanofibril papers and their bionanocomposites: a review. Carbohydr Polym 273:118507. https://doi.org/10.1016/j.carbpol.2021.118507

Mulakkal MC, Trask RS, Ting VP, Seddon AM (2018) Responsive cellulose-hydrogel composite ink for 4D printing. Mater Des 160:108–118. https://doi.org/10.1016/j.matdes.2018.09.009

Oh SY, Dong IY, Shin Y et al (2005) Crystalline structure analysis of cellulose treated with sodium hydroxide and carbon dioxide by means of X-ray diffraction and FTIR spectroscopy. Carbohydr Res 340:2376–2391. https://doi.org/10.1016/j.carres.2005.08.007

Peng N, Huang D, Gong C et al (2020) Controlled arrangement of Nanocellulose in Polymeric Matrix: from reinforcement to functionality. ACS Nano 14:16169–16179. https://doi.org/10.1021/acsnano.0c08906

Reid MS, Villalobos M, Cranston ED (2016) Cellulose nanocrystal interactions probed by thin film swelling to predict dispersibility. Nanoscale 8:12247–12257. https://doi.org/10.1039/c6nr01737a

Saito T, Isogai A (2004) TEMPO-Mediated oxidation of native cellulose. The Effect of Oxidation Conditions on Chemical and Crystal Structures of the water-insoluble fractions. Biomacromolecules 5:1983–1989. https://doi.org/10.1021/bm0497769

Saito T, Shibata I, Isogai A et al (2005) Distribution of carboxylate groups introduced into cotton linters by the TEMPO-mediated oxidation. Carbohydr Polym 61:414–419. https://doi.org/10.1016/j.carbpol.2005.05.014

Schwanninger M, Rodrigues JC, Pereira H, Hinterstoisser B (2004) Effects of short-time vibratory ball milling on the shape of FT-IR spectra of wood and cellulose. Vib Spectrosc 36:23–40. https://doi.org/10.1016/j.vibspec.2004.02.003

Segal L, Creely JJ, Martin AE, Conrad J CM (1959) An empirical method for estimating the degree of crystallinity of native cellulose using the X-Ray diffractometer. Text Res J 29:786–794. https://doi.org/10.1177/004051755902901003

Smallwood IM (2012) Handbook of organic solvent properties. pp 1–306. https://doi.org/10.1016/C2009-0-23646-4

Srinivasan AV, Haritos GK, Hedberg FL (1991) Biomimetics: advancing man-made materials through guidance from nature. Appl Mech Rev 44:463–482. https://doi.org/10.1115/1.3119489

Venkatram S, Kim C, Chandrasekaran A, Ramprasad R (2019) Critical assessment of the hildebrand and hansen

solubility parameters for polymers. J Chem Inf Model. https://doi.org/10.1021/acs.jcim.9b00656

Wågberg L, Decher G, Norgren M et al (2008) The build-up of polyelectrolyte multilayers of microfibrillated cellulose and cationic polyelectrolytes. Langmuir 24:784–795. https://doi.org/10.1021/la702481v

Wang M, Tian X, Ras RHA, Ikkala O (2015) Sensitive humidity-driven reversible and bidirectional bending of nanocellulose thin films as bio-inspired actuation. Adv Mater Interfaces 2:1500080. https://doi.org/10.1002/admi.201500080

Wang X, Huang H, Liu H et al (2019) Multi-Responsive Bilayer Hydrogel Actuators with programmable and precisely tunable motions. Macromol Chem Phys 220:1–8. https://doi.org/10.1002/macp.201800562

Wang L, Li K, Copenhaver K et al (2021) Review on nonconventional fibrillation methods of producing cellulose nanofibrils and their applications. Biomacromolecules 22:4037–4059. https://doi.org/10.1021/acs.biomac.1C00640

Wei J, Jia S, Guan J et al (2021) Robust and highly sensitive cellulose nanofiber-based humidity actuators. ACS Appl Mater Interfaces 13:54417–54427. https://doi.org/10.1021/acsami.1c17894

Yang L, Cui J, Zhang L et al (2021) A moisture-driven actuator based on polydopamine-modified MXene/bacterial cellulose nanofiber composite film. Adv Funct Mater 31:1–11. https://doi.org/10.1002/adfm.202101378

Zhang L, Chizhik S, Wen Y, Naumov P (2016) Directed motility of hygroresponsive biomimetic actuators. Adv Funct Mater 26:1040–1053. https://doi.org/10.1002/adfm.201503922

Zhang X, Yu Y, Jiang Z, Wang H (2016b) Influence of thickness and moisture content on the mechanical properties of microfibrillated cellulose (MFC) films. Wood Res 61:851–860

Zhao Q, Liang Y, Ren L et al (2018) Design and fabrication of nanofibrillated cellulose-containing bilayer hydrogel actuators with temperature and near infrared laser responses. J Mater Chem B 6:1260–1271. https://doi.org/10.1039/c7tb02853a

Zhao Q, Chang Y, Yu Z et al (2020) Bionic intelligent soft actuators: high-strength gradient intelligent hydrogels with diverse controllable deformations and movements. J Mater Chem B 8:9362–9373. https://doi.org/10.1039/d0tb01927e

Zhou S, Zhou S, Zhou Q et al (2020) Design and preparation of 3D printing intelligent poly N,N-dimethylacrylamide hydrogel actuators. E-Polymers 20:273–281. https://doi.org/10.1515/epoly-2020-0033